Supporting Information

Experimental results for arginine kinase

For the 42 kDa protein arginine kinase (AK), it took over a week to measure relaxation parameters by traditional spin relaxation experiments. Here, we aim to acquire data of the same quality in less time using CEST-based experiments. Apo-AK data was recorded at 25°C and pH 6.5 on a Bruker Avance IIIHD 800 MHz instrument equipped with a TXI CryoProbe. ^{15}N CEST experiments were recorded for two B_1 fields (30 Hz and 60 Hz) as described previously [1] with the ^{1}H (^{15}N) carrier set to 4.79 (118.3) ppm, a sweep width of 20.0 (26.3) ppm, and accumulation 1536* (108*) complex points resulting in an acquisition time of 95.8 (50.6) ms. A total of 67 (45) B_1 offsets over the range of 97 to 137 ppm were used for data acquired with 30 (60) Hz B_1 field strength. A recycle delay of 1.5 sec was used with 4 transients per FID and a CEST mixing time (T_{rlx}) of 0.8 seconds. Together, the total time required to acquire the two datasets was approximately 39 and 26.5 hours for B_1 fields of 30 and 60 Hz, respectively. Calibration of the B_1 fields was performed as described previously[1] using the approach of Guenneugues, *et al.*[2] by placing the ^{15}N carrier on an isolated resonance (here an isolated tryptophan side-chain signal) and incrementing T_{rlx} to obtain an FID. The oscillation frequency, obtained from Fourier transformation or numerical fitting, provides the actual B_1 field value. The 30 (60) Hz B_1 field was determined as 32.7 ± 0.2 (64.3 ± 0.3) Hz. These values are then used in the analysis of the CEST profiles using ChemEx.[1]

An increase in R_1 and concomitant decrease in R_2 at the substrate-binding loop L8 (V308-V322) was detected by both types of experiments reflecting large amplitude loop motions as reported previously.[3] The largest discrepancy between CEST and regular spin relaxation measurements is observed for R_2 values of certain residues: CEST-derived rates of the three residues R193, T197 and A200 belonging to loop L8 show a substantial increase, which can be attributed to a slow conformational exchange process that may facilitate substrate binding.[3] A uniform elevation of R_1 by 5% and a reduction of R_2 by 6% measured by CEST are likely due to a systematic difference in temperature between the two sets of measurements. Despite the small systematic offset in R_1 and R_2, the S^2

order parameters derived from CEST and the L-MFA method are very similar to the ones derived from regular spin relaxation experiments.

NMR data analysis

All spectra were processed using the NMRPipe suite of programs,[4] with intensities extracted for CEST profiles using the nlinLS lineshape fitting alogorithm. This is an important step as it fixes lineshape parameters across all CEST planes, improving the accuracy of the extracted intensities even for overlapped and weak resonances. Analysis of the CEST profiles was performed using the ChemEx program (https://github.com/gbouvignies/chemex), which numerically integrates the Bloch-McConnell equations[5] describing chemical exchange, as explained previously.[1] In this work, analysis assuming one- or two-sites (conformational states) was performed on all residues. For single-site analysis (i.e. in the absence of exchange), values of k_{ex} , p_B , $\Delta\omega$, and ΔR_2 are fixed at 0 while only R_1, R_2, and I_0 (the reference intensity when no saturating B_1 field is applied) are fit for each residue. For two-site exchange, the above fixed values are also fit, with the exception of ΔR_2, which is only fit when more than one B_1 field is being analyzed. This is due to a strong correlation between k_{ex} and ΔR_2 that cannot be separated with a single B_1 field. By contrast, the fitting of R_1 and R_2 of the ground-state is stable using CEST data at a single B_1 field as is discussed below.

Traditional ^{15}N spin relaxation experiments

Backbone amide ^{15}N R_1 and $R_{1\rho}$ experiments were acquired according to the in-phase experiments of Lakomek, et al.[6] with a small modification to saturate proton signals of the protein while preserving water magnetization following the acquisition of each FID.[7] Saturation of protein signals ensures that identical magnetization buildup occurs during each scan, independent of the relaxation mixing time, while preserving the water magnetization minimizes the contribution of amide proton exchange to the relaxation rates. Rates recorded in this fashion with inter-scan delays of 1.5 or 5.0 sec were identical. Ubiquitin data was recorded at 25°C and pH 7.0 on a Bruker Avance IIIHD 850 MHz instrument equipped with a TCI cryoprobe. The ^{1}H (^{15}N) carrier set to 4.79 (117.6) ppm, a sweep width of 16.0 (22.0) ppm, and accumulation 1024* (48*) complex points

resulting in an acquisition time of 106.5 (35.9) ms. For each experiment, 7 relaxation times were recorded: 40, 240, 640, 800 (x 2), and 1000 (x 2) ms for R_1 and 2, 12, 25 (x 2), 56, 94 (x 2) ms for $R_{1\rho}$. The B_1 field used for the $R_{1\rho}$ experiment was calibrated by measuring the offset-dependence of $^1J_{NH}$ couplings in the presence of the spinlock[8] and found to be 1999.2 ± 1.0 Hz. Errors in R_1 and $R_{1\rho}$ were determined using the covariance method of the exponential fits of the data. Values of R_2 were calculated from $R_{1\rho}$ values according to:

$$R_{1\rho} = R_1\cos^2(\theta) + R_2\sin^2(\theta) \quad (1)$$

where θ is the tilt angle of the effective magnetic field in the rotating frame, $\tan(\theta) = \frac{\omega_1}{\Omega}$, ω_1 is the spinlock field strength, and Ω is the resonance offset from the spinlock carrier frequency. Errors in R_2 were determined by standard error propagation of R_1, $R_{1\rho}$, and ω_1 uncertainties.

The R_1, R_2, NOE data of apo-AK at 800 MHz were taken from the literature.[3]

Robustness of CEST-derived of R_1 and R_2 values

It is well understood that to extract accurate conformational exchange parameters from CEST profiles, multiple B_1 fields are required.[9] However, little is known about the accuracy of ground-state relaxation parameters extracted from CEST profiles. While small B_1 fields are usually necessary to observe the minor state dips resulting from exchange processes, these require many more B_1 offsets to acquire a full CEST profile as the offset step-size is typically of the order of the B_1 field itself. Using larger B_1 fields can therefore reduce the experimental time significantly, albeit with broader profiles and thus less sensitivity to exchange. Here, we recorded CEST profiles for ubiquitin at two B_1 fields, 25 and 100 Hz, and explored whether the R_1 and R_2 values extracted using CEST data from one or both B_1 fields is more accurate. Ubiquitin data was recorded at 25°C and pH 7.0 on a Bruker Avance IIIHD 850 MHz instrument equipped with a TCI cryprobe. CEST experiments were recorded as described above for apo-AK, with carrier, sweep width, complex points, and acquisition times of 4.79 (120.8) ppm, 16.0 (18.5) ppm, 1024* (64*), and 75.4 (40.2) ms for proton (nitrogen), respectively. The CEST frequency sweep spanned 100 to 140 ppm with 116 offsets (plus a reference) for the B_1 of 25 Hz,

and from 92 to 150 ppm with 41 offsets (plus a reference) for the 100 Hz B_1 field. With a recycle delay of 1.5 sec, T_{rlx} of 450 ms, and 2 transients per FID, CEST experiments were acquired in approximately 16.6 and 6.0 hours for 25 and 100 Hz B_1 fields, respectively. Calibration of the B_1 fields found values of 26.3 ± 0.1 Hz and 105.8 ± 0.5 Hz, with inhomogeneity of the field determined to be about 10%. From the analysis of these datasets, we found no significant effect on R_1, whereas R_2 extracted from the larger of the two CEST B_1 fields (100 Hz) shows a better correlation (R = 0.98) than the one from the smaller B_1 field at 25 Hz (R = 0.66) compared to R_2 data measured by regular spin relaxation experiments at 850 MHz magnetic field strength.

Sensitivity and robustness analysis of CEST-derived R_1 and R_2 parameters

For a more systematic analysis, we generated numerous two-site exchange CEST profiles as a function of k_{ex}, p_B, $\Delta\omega$, and ΔR_2, with 0.5% Gaussian intensity noise relative to the reference dataset, and subsequently fit these profiles using ChemEx assuming the absence ("− Exch") or presence ("+ Exch") of two-site exchange (Tables S1-S4). Of note, the change in R_1 between the ground and excited states (ΔR_1) is set to 0 s^{-1} for all simulations as CEST profiles are largely insensitive to this parameter.[9b, 10] Analysis of the simulation results confirms that the extraction of R_1 from CEST data at a single field is highly robust, independent of whether exchange is assumed or not. The largest discrepancies in R_1 occur when large populations of an excited state are present (Table S4). However, in these cases the minor state dip is obvious from the CEST profile and accurate ground-state R_1 values can again be obtained by fitting the exchange contribution.

Qualitatively different results are observed for the extraction of the ground state R_2 value from CEST profiles with several trends being notable. First, when a single-state model is assumed ("− Exch"), larger B_1 fields are required to suppress exchange contributions and obtain accurate R_2 values. This is analogous to $R_{1\rho}$ experiments where the largest B_1 fields are often used to suppress as much exchange as possible. Second, the use of multiple B_1 fields in single-state fitting does not necessarily improve the accuracy of the extracted R_2 values. However, the inconsistency in the results and poor fitting (reduced $\chi^2 > 1$) can be indicative of the presence of exchange when no significant minor state dip is observed. Third, when the presence of exchange can be identified, either by

poor fitting or an observable minor dip, accurate R_2 values can once again be obtained by including the exchange contribution in the fitting ("+ Exch"). This is true even for single-field fits of the data despite significant uncertainty in the global exchange parameters (not shown). The only exception to this occurs at large values of k_{ex} (Table S3, 10,000 s^{-1}). Here, the error in the extracted R_2 values is relatively large even with a fitting error that is relatively small (reduced $\chi^2 \approx 1$). In these cases, the observed increase in extracted R_2 without a concomitant decrease in R_1 is a signature for residues experiencing exchange when compared with other residues in the protein. Such exchanging residues should be excluded from a subsequent L-MFA analysis.

ΔR_2 (s^{-1})	Fitting	B_1 Fields	R_1 (s^{-1})	σ_{R1}	R_2 (s^{-1})	σ_{R2}	Red. χ^2	$\sigma_{\chi 2}$
0	− Exch	25	1.546	0.011	10.61	0.15	16.9	6.1
	− Exch	100	1.477	0.011	13.98	0.21	6.4	3.1
	− Exch	500	**1.499**	**0.011**	**10.15**	**0.15**	**0.8**	**0.3**
	− Exch	25,100	1.525	0.011	11.71	0.36	15.2	4.2
	+ Exch	25	**1.500**	**0.011**	**10.03**	**0.39**	**0.7**	**0.2**
	+ Exch	100	**1.501**	**0.012**	**10.26**	**0.66**	**0.5**	**0.2**
	+ Exch	25,100	**1.500**	**0.008**	**10.00**	**0.14**	**0.7**	**0.2**
10	− Exch	25	1.547	0.010	10.60	0.15	17.2	5.9
	− Exch	100	1.478	0.012	14.08	0.22	7.0	3.2
	− Exch	500	**1.498**	**0.012**	10.27	0.15	**0.8**	**0.3**
	− Exch	25,100	1.526	0.011	11.80	0.39	15.9	4.3
	+ Exch	25	**1.500**	**0.011**	**10.06**	**0.43**	**0.7**	**0.2**
	+ Exch	100	**1.501**	**0.012**	**10.23**	**0.62**	**0.6**	**0.2**
	+ Exch	25,100	**1.500**	**0.008**	**10.01**	**0.14**	**0.7**	**0.2**
100	− Exch	25	1.556	0.011	10.56	0.16	17.1	5.8
	− Exch	100	1.485	0.012	14.74	0.23	7.8	3.2
	− Exch	500	**1.500**	**0.012**	11.07	0.17	**0.8**	**0.3**
	− Exch	25,100	1.536	0.011	11.91	0.43	17.0	4.4
	+ Exch	25	**1.500**	**0.011**	**10.03**	**0.40**	**0.8**	**0.2**
	+ Exch	100	**1.501**	**0.012**	**10.09**	**0.51**	**0.6**	**0.2**
	+ Exch	25,100	**1.500**	**0.008**	**10.00**	**0.15**	**0.7**	**0.2**
1000	− Exch	25	1.560	0.011	10.76	0.15	5.7	2.1
	− Exch	100	1.551	0.012	15.74	0.28	15.5	7.5
	− Exch	500	1.535	0.012	14.91	0.24	3.0	1.4
	− Exch	25,100	1.568	0.008	12.43	0.54	13.9	4.7
	+ Exch	25	**1.500**	**0.013**	**10.02**	**0.54**	**0.8**	**0.2**
	+ Exch	100	**1.501**	**0.015**	**10.00**	**0.58**	**0.8**	**0.3**
	+ Exch	25,100	**1.499**	**0.009**	**10.00**	**0.16**	**0.8**	**0.2**

Table S1. Monte Carlo CEST simulation results as a function of ΔR_2. True values of R_1 and R_2 are 1.5 s^{-1} and 10.0 s^{-1}, respectively. 1000 simulated datasets were produced with k_{ex} = 100 s^{-1}, p_B = 1.0%, $\Delta\omega$ = 400 Hz, ΔR_2 as indicated in the left column, and 0.5% error intensity error (with respect to the reference dataset) for B_1 values of 25, 100, and 500 Hz. Individual B_1 fields, or combinations of B_1 fields, were then fit with ChemEx assuming the absence of conformational exchange ("− Exch" : $k_{ex} = p_B = \Delta\omega = \Delta R_2 = 0$, and only I_0, R_1, and R_2 are fit), or the presence of exchange ("+ Exch"), where k_{ex}, p_B, $\Delta\omega$, and ΔR_2 are also fit. **Bold values** are within error of the true values.

$\Delta\varpi$ (Hz)	Fitting	B_1 Fields	R_1 (s^{-1})	σ_{R1}	R_2 (s^{-1})	σ_{R2}	Red. χ^2	$\sigma_{\chi 2}$
0	− Exch	25	**1.500**	**0.011**	**10.00**	**0.14**	**0.8**	**0.3**
	− Exch	100	**1.500**	**0.011**	**9.99**	**0.15**	**0.7**	**0.3**
	− Exch	500	**1.500**	**0.011**	**10.01**	**0.15**	**0.8**	**0.3**
	− Exch	25,100	**1.500**	**0.008**	**9.99**	**0.11**	**0.8**	**0.2**
	+ Exch	25	**1.499**	**0.011**	**9.96**	**0.19**	**0.9**	**0.3**
	+ Exch	100	**1.505**	**0.011**	**9.55**	**1.13**	**0.8**	**0.4**
	+ Exch	25,100	**1.497**	**0.008**	10.22	0.18	1.6	0.5
40	− Exch	25	**1.496**	**0.011**	10.60	0.15	**0.9**	**0.3**
	− Exch	100	**1.500**	**0.011**	**10.03**	**0.16**	**0.7**	**0.3**
	− Exch	500	**1.500**	**0.011**	**10.00**	**0.15**	**0.8**	**0.3**
	− Exch	25,100	**1.497**	**0.008**	10.35	0.14	**0.9**	**0.2**
	+ Exch	25	**1.496**	**0.011**	**10.21**	**0.80**	**1.0**	**0.4**
	+ Exch	100	**1.504**	**0.011**	**9.83**	**0.49**	**0.7**	**0.2**
	+ Exch	25,100	**1.494**	**0.008**	10.56	0.19	1.6	0.4
80	− Exch	25	**1.490**	**0.011**	12.37	0.17	1.9	0.7
	− Exch	100	**1.498**	**0.011**	**10.16**	**0.15**	**0.7**	**0.3**
	− Exch	500	**1.500**	**0.011**	**10.01**	**0.16**	**0.8**	**0.3**
	− Exch	25,100	1.491	0.008	11.34	0.29	2.1	0.6
	+ Exch	25	**1.500**	**0.011**	**10.02**	**0.48**	**0.9**	**0.6**
	+ Exch	100	**1.501**	**0.010**	**9.86**	**0.27**	**0.7**	**0.2**
	+ Exch	25,100	1.490	0.009	11.46	0.45	4.0	1.4
200	− Exch	25	1.518	0.011	12.27	0.18	14.5	5.1
	− Exch	100	1.487	0.011	11.34	0.16	1.2	0.5
	− Exch	500	**1.499**	**0.011**	**10.03**	**0.15**	**0.8**	**0.3**
	− Exch	25,100	1.502	0.009	11.79	0.17	9.6	3.1
	+ Exch	25	**1.500**	**0.011**	**10.01**	**0.22**	**0.7**	**0.2**
	+ Exch	100	**1.499**	**0.011**	**9.98**	**0.37**	**0.7**	**0.4**
	+ Exch	25,100	**1.499**	**0.008**	**10.09**	**0.16**	**1.1**	**0.3**

Table S2. Monte Carlo CEST simulation results as a function of $\Delta\omega$. True values of R_1 and R_2 are 1.5 s^{-1} and 10.0 s^{-1}, respectively. 1000 simulated datasets were produced with k_{ex} = 100 s^{-1}, p_B = 1.0%, ΔR_2 = 0 s^{-1}, $\Delta\omega$ as indicated in the left column, and 0.5% error intensity error (with respect to the reference dataset) for B_1 values of 25, 100, and 500 Hz. Individual B_1 fields, or combinations of B_1 fields, were then fit with ChemEx assuming the absence of conformational exchange ("− Exch" : $k_{ex} = p_B = \Delta\omega = \Delta R_2 = 0$, and only I_0, R_1, and R_2 are fit), or the presence of exchange ("+ Exch"), where k_{ex}, p_B, and $\Delta\omega$ are also fit. **Bold values** are within error of the true values. Values for $\Delta\omega$ = 400 Hz can be found in Table S1, $\Delta R_2 = 0$.

k_{ex} (s^{-1})	Fitting	B_1 Fields	R_1 (s^{-1})	σ_{R1}	R_2 (s^{-1})	σ_{R2}	Red. χ^2	$\sigma_{\chi 2}$
20	− Exch	25	1.513	0.011	**10.01**	**0.14**	2.4	0.9
	− Exch	100	**1.498**	**0.011**	10.73	0.16	**1.3**	**0.7**
	− Exch	500	**1.500**	**0.011**	**10.04**	**0.15**	**0.8**	**0.3**
	− Exch	25,100	**1.507**	**0.008**	10.31	0.14	2.1	0.7
	+ Exch	25	**1.500**	**0.011**	**10.04**	**0.20**	**0.8**	**0.3**
	+ Exch	100	**1.500**	**0.011**	**10.01**	**0.20**	**0.7**	**0.3**
	+ Exch	25,100	**1.499**	**0.008**	**10.02**	**0.14**	**0.7**	**0.2**
500	− Exch	25	1.563	0.011	15.04	0.21	23.2	8.4
	− Exch	100	1.407	0.012	23.59	0.26	11.1	4.5
	− Exch	500	**1.493**	**0.011**	10.67	0.15	**0.9**	**0.4**
	− Exch	25,100	**1.518**	**0.018**	17.77	0.90	35.0	9.8
	+ Exch	25	**1.500**	**0.011**	**10.00**	**0.19**	**0.7**	**0.2**
	+ Exch	100	**1.499**	**0.011**	**10.01**	**0.23**	**0.6**	**0.2**
	+ Exch	25,100	**1.499**	**0.008**	**9.99**	**0.14**	**0.6**	**0.2**
2,500	− Exch	25	**1.504**	**0.011**	23.31	0.28	3.7	1.3
	− Exch	100	1.431	0.012	23.93	0.29	4.7	2.2
	− Exch	500	1.479	0.011	12.25	**0.17**	**1.7**	**0.8**
	− Exch	25,100	1.474	0.012	23.35	0.20	10.1	3.6
	+ Exch	25	**1.500**	**0.012**	**9.89**	**2.92**	**0.9**	**0.3**
	+ Exch	100	**1.500**	**0.012**	**9.92**	**1.22**	**0.8**	**0.3**
	+ Exch	25,100	**1.500**	**0.008**	**9.94**	**0.82**	**0.9**	**0.2**
10,000	− Exch	25	**1.500**	**0.010**	16.05	0.20	**0.9**	**0.3**
	− Exch	100	**1.489**	**0.011**	15.94	0.21	**0.8**	**0.3**
	− Exch	500	1.476	0.011	13.43	0.19	**1.3**	**0.6**
	− Exch	25,100	**1.495**	**0.008**	15.99	0.15	**0.9**	**0.2**
	+ Exch	25	**1.500**	**0.011**	**13.65**	**4.43**	**0.8**	**0.3**
	+ Exch	100	**1.497**	**0.014**	**11.99**	**3.87**	**0.7**	**0.3**
	+ Exch	25,100	**1.499**	**0.009**	**11.30**	**4.09**	**0.8**	**0.2**

Table S3. Monte Carlo CEST simulation results as a function of k_{ex}. True values of R_1 and R_2 are 1.5 s^{-1} and 10.0 s^{-1}, respectively. 1000 simulated datasets were produced with p_B = 1.0%, ΔR_2 = 0 s^{-1}, $\Delta\omega$ = 400 Hz, k_{ex} as indicated in the left column, and 0.5% error intensity error (with respect to the reference dataset) for B_1 values of 25, 100, and 500 Hz. Individual B_1 fields, or combinations of B_1 fields, were then fit with ChemEx assuming the absence of conformational exchange ("− Exch" : $k_{ex} = p_B = \Delta\omega = \Delta R_2 = 0$, and only I_0, R_1, and R_2 are fit), or the presence of exchange ("+ Exch"), where k_{ex}, p_B, and $\Delta\omega$ are also fit. **Bold values** are within error of the true values. Values for k_{ex} = 100 s^{-1} can be found in Table S1, $\Delta R_2 = 0$.

p_B (%)	Fitting	B_1 Fields	R_1 (s^{-1})	σ_{R1}	R_2 (s^{-1})	σ_{R2}	Red. χ^2	$\sigma_{\chi 2}$
0	− Exch	25	**1.500**	**0.010**	**10.00**	**0.14**	**0.8**	**0.3**
	− Exch	100	**1.500**	**0.011**	**10.01**	**0.15**	**0.7**	**0.3**
	− Exch	500	**1.500**	**0.011**	**10.00**	**0.15**	**0.8**	**0.3**
	− Exch	25,100	**1.500**	**0.008**	**10.00**	**0.11**	**0.8**	**0.2**
	+ Exch	25	**1.500**	**0.003**	**10.00**	**0.03**	**1.0**	**0.4**
	+ Exch	100	**1.500**	**0.003**	**9.90**	**0.92**	**0.9**	**0.5**
	+ Exch	25,100	**1.500**	**0.003**	**9.97**	**0.29**	**0.9**	**0.3**
5	− Exch	25	1.670	0.011	13.52	0.20	150.6	53.3
	− Exch	100	1.391	0.012	25.77	0.30	13.3	5.3
	− Exch	500	**1.493**	**0.012**	10.69	0.17	**0.9**	**0.4**
	− Exch	25,100	1.569	0.032	18.08	1.48	116.2	31.4
	+ Exch	25	**1.500**	**0.011**	**10.01**	**0.29**	**0.7**	**0.2**
	+ Exch	100	**1.500**	**0.012**	**10.01**	**0.43**	**0.6**	**0.2**
	+ Exch	25,100	**1.500**	**0.008**	**10.03**	**0.20**	**0.6**	**0.1**
10	− Exch	25	1.749	0.012	18.12	0.32	260.8	87.3
	− Exch	100	1.363	0.013	31.16	0.34	16.5	6.3
	− Exch	500	**1.488**	**0.012**	11.22	0.18	**1.1**	**0.5**
	− Exch	25,100	1.575	0.049	24.89	1.97	191.8	55.5
	+ Exch	25	**1.500**	**0.012**	**10.00**	**0.48**	**0.7**	**0.2**
	+ Exch	100	**1.500**	**0.013**	**9.92**	**0.74**	**0.7**	**0.2**
	+ Exch	25,100	**1.500**	**0.009**	**10.01**	**0.32**	**0.7**	**0.2**
25	− Exch	25	1.067	0.015	257.58	2.26	193.1	68.2
	− Exch	100	1.331	0.015	38.98	0.47	14.0	6.1
	− Exch	500	1.480	0.014	12.19	0.22	**1.3**	**0.6**
	− Exch	25,100	1.435	0.125	63.26	36.54	207.4	60.0
	+ Exch	25	**1.499**	**0.015**	**10.08**	**1.29**	**0.8**	**0.3**
	+ Exch	100	**1.499**	**0.017**	**10.08**	**1.51**	**0.7**	**0.3**
	+ Exch	25,100	**1.499**	**0.011**	**9.99**	**0.58**	**0.8**	**0.2**

Table S4. Monte Carlo CEST simulation results as a function of p_B. True values of R_1 and R_2 are 1.5 s^{-1} and 10.0 s^{-1}, respectively. 1000 simulated datasets were produced with k_{ex} = 100 s^{-1}, ΔR_2 = 0 s^{-1}, $\Delta\omega$ = 400 Hz, p_B as indicated in the left column, and 0.5% error intensity error (with respect to the reference dataset) for B_1 values of 25, 100, and 500 Hz. Individual B_1 fields, or combinations of B_1 fields, were then fit with ChemEx assuming the absence of conformational exchange ("− Exch" : $k_{ex} = p_B = \Delta\omega = \Delta R_2 = 0$, and only I_0, R_1, and R_2 are fit), or the presence of exchange ("+ Exch"), where k_{ex}, p_B, and $\Delta\omega$ are also fit. **Bold values** are within error of the true values. Values for p_B = 1% can be found in Table S1, $\Delta R_2 = 0$.

Molecular Dynamics (MD) simulations and back-calculation of relaxation parameters

Molecular dynamics (MD) simulations were performed using the protocol reported previously[11] for 10 proteins with variable size and topologies with their initial 3D structures taken from the PDB (PDB codes 1MJC, 1EKG, 1GNU, 1GST, 1QZM, 1VYK, 2B02, 2END, 1IGD, and 1UBI). From each trajectory R_1, R_2 and NOE values were computed following Eqs. 1-7 of Ref.[11] Briefly, for each ^{15}N-^{1}H bond vector, the spectral density function $J(\omega)$ was determined by Fourier transformation of the multi-exponentially decaying reorientational correlation function composed of both the internal correlation function and the overall tumbling correlation function. The relaxation parameters were then calculated as a linear combination of spectral density functions sampled at the Larmor frequencies, ω_N and ω_H, and their sum and difference:

$$R_1 = 1/T_1 = d_{oo}\left[3J(\omega_N) + J(\omega_H - \omega_N) + 6J(\omega_N + \omega_N)\right] + c_{oo}\omega_N^2 J(\omega_N) \quad (2)$$

$$R_2 = 1/T_2 = \frac{1}{2}d_{oo}\left[4J(0) + 3J(\omega_N) + J(\omega_H - \omega_N) + 6J(\omega_H) + 6J(\omega_N + \omega_H)\right] + \frac{1}{6}c_{oo}\omega_N^2\left[4J(0) + 3J(\omega_N)\right] \quad (3)$$

where the N-H bond length was set to be 1.02 Å and the ^{15}N chemical shielding anisotropy (CSA) was set to -160 ppm for model-free fitting of both MD-derived and experimentally measured ^{15}N R_1, R_2 and NOE.

Lean model-free (L-MFA) and regular model-free analysis (MFA)

The model-free approach (MFA) and the simplified L-MFA were applied to either the MD-derived or experimentally measured R_1, R_2, and NOE parameters. The difference between MFA and L-MFA is the number of relaxation parameters as input. While at a given B_0 field MFA takes into account all three relaxation parameters, L-MFA uses only the R_1 and R_2 relaxation rates. Both MFA and L-MFA were applied to globular proteins assuming isotropic tumbling. The τ_c was fixed at either a predefined or estimated value and two parameters (S^2 and τ_{int}) were fitted to the model described below. Internal motional correlation function $C_I(t)$ and the corresponding spectral density function $J(\omega)$ after Fourier transformation are:

$$C_1(t) = S^2 + (1 - S^2)\ e^{-t/\tau_{\text{int}}} \tag{4}$$

$$J(\omega) = S^2 \frac{2\tau_c}{1 + (\omega\ \tau_c)^2} + (1 - S^2) \frac{2\tau_{eff}}{1 + (\omega\ \tau_{eff})^2} \tag{5}$$

where $\tau_{eff} = \tau_c \tau_{\text{int}} / (\tau_c + \tau_{\text{int}})$. The generalized order parameters S^2 and τ_{int} were obtained by non-linear least square minimization of the target function. Monte Carlo (MC) error analysis was performed by fitting model-free parameters after adding 5% random errors to each relaxation parameter. The error bars were determined as the standard deviations of the fitted order parameters over 30 Monte Carlo simulations. The model-free analysis was performed using in-house MATLAB scripts. The global tumbling correlation time τ_c values were estimated as a function of τ_c calculated from R_2/R_1 ratio over all ^{15}N sites that are part of well-defined secondary structures, i.e. α-helices and β-strands, and hence exhibit only moderate internal dynamics with fast internal correlation times τ_{int}. The spectra density function then simplifies to $J(\omega) = 2S^2\tau_c / (1+\omega^2\ \tau_c^2)$ and R_1 and R_2 parameters are computed with this $J(\omega)$ using Eqs. 2 - 3. After translating each ^{15}N R_2/R_1 ratio into a residue-wise τ_c, a global tumbling correlation time τ_c^{est} is obtained from the average of the τ_c distribution of residues that are part of well-defined secondary structures, which yields a stable estimate for the global τ_c (see Figure S13).

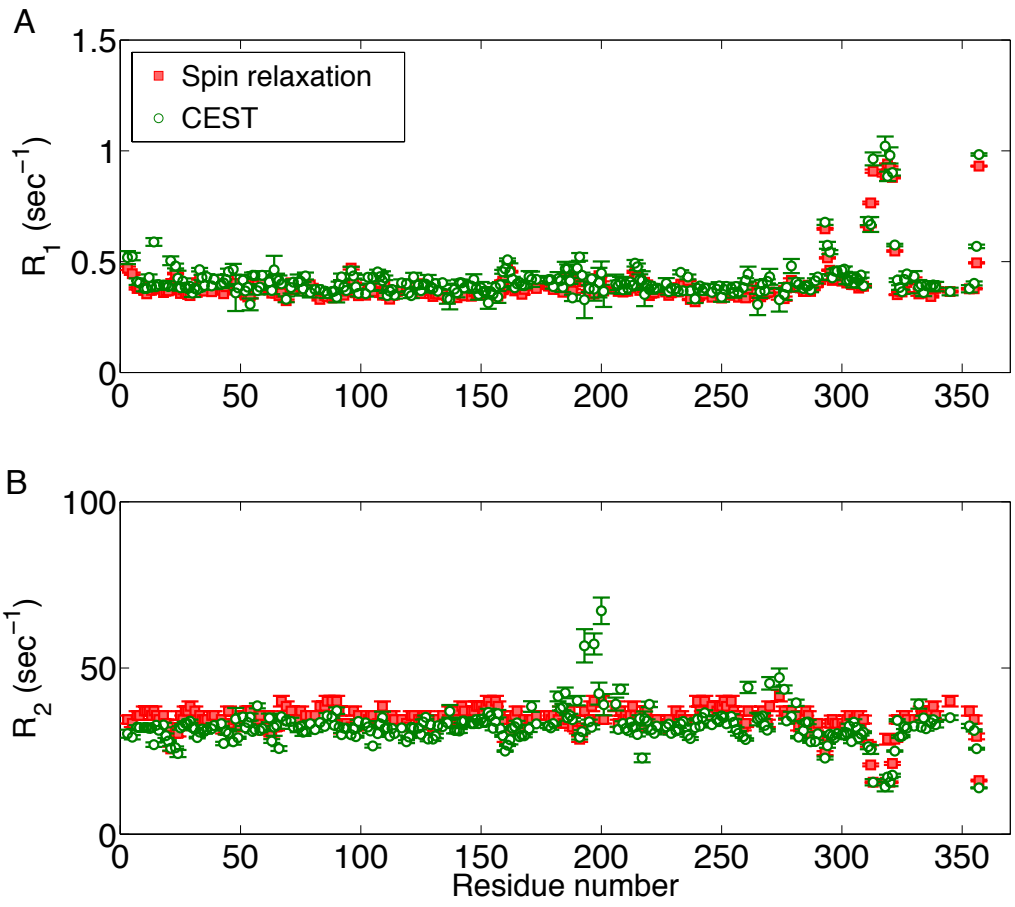

Figure S1. Comparison of experimental relaxation parameters (A) R_1 and (B) R_2 of arginine kinase (AK) derived from CEST (green circles) and standard spin relaxation experiments (red squares) at 800 MHz magnetic field strength. A uniform elevation of R_1 by 5% and a reduction of R_2 by 6% measured by CEST are likely due to a small difference in temperature between the two sets of measurements.

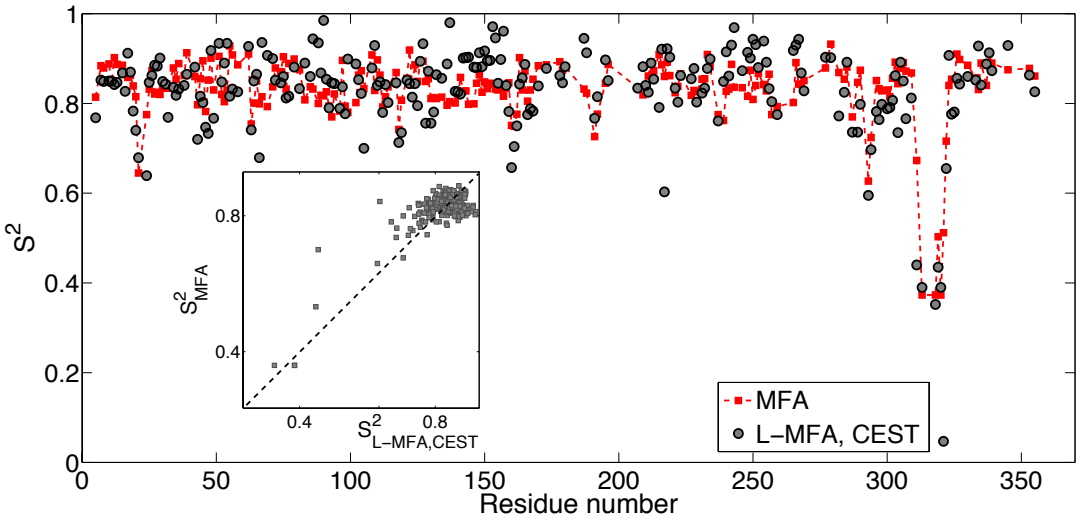

Figure S2. Comparison of AK order parameters S^2_{LMFA} determined from CEST-derived R_1, R_2 values (black circles) and previously reported S^2_{MFA} determined from R_1, R_2 and NOE data of standard spin relaxation experiments (red squares). The inset shows a correlation plot for the two types of order parameters.

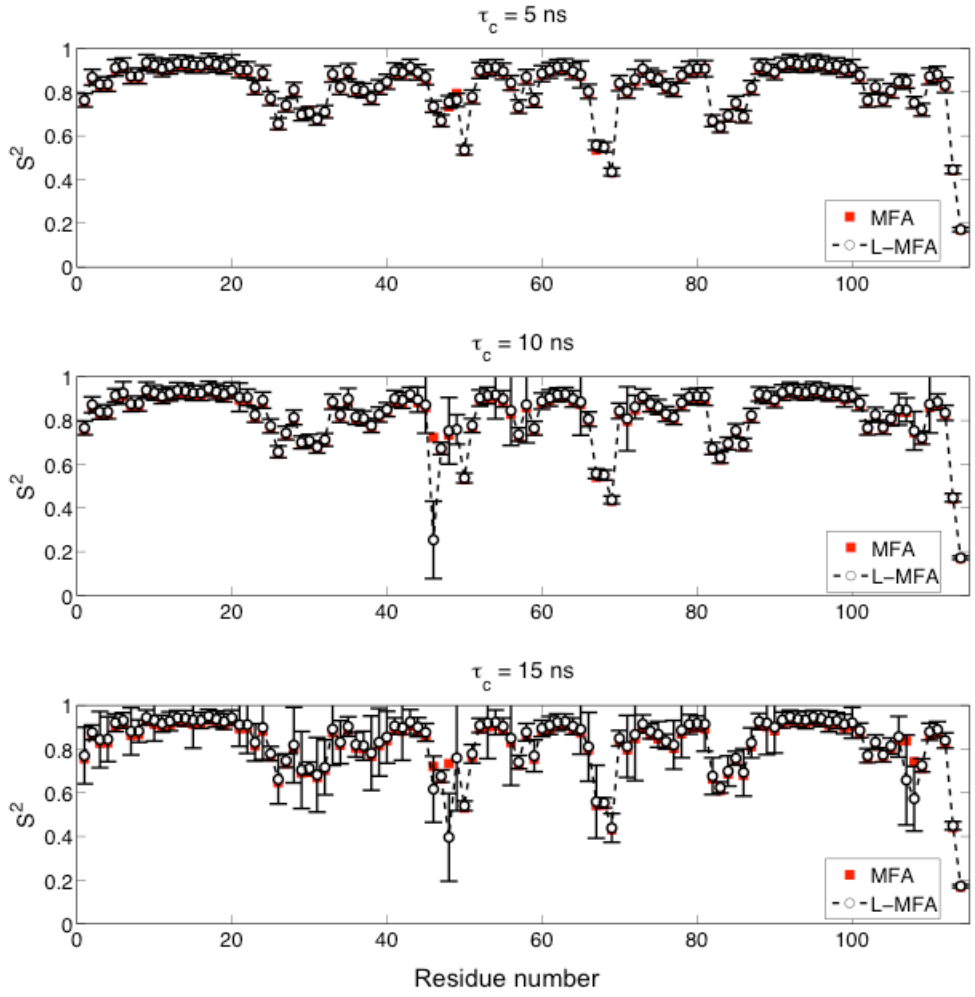

Figure S3. Comparison of S^2 order parameters determined by MFA and L-MFA methods with different τ_c values of 5 ns, 10 ns and 15 ns (from top to bottom). The error bars were estimated by Monte Carlo simulations with 5% errors for R_1 and R_2 values extracted from the MD trajectory (PDB: 1EKG).

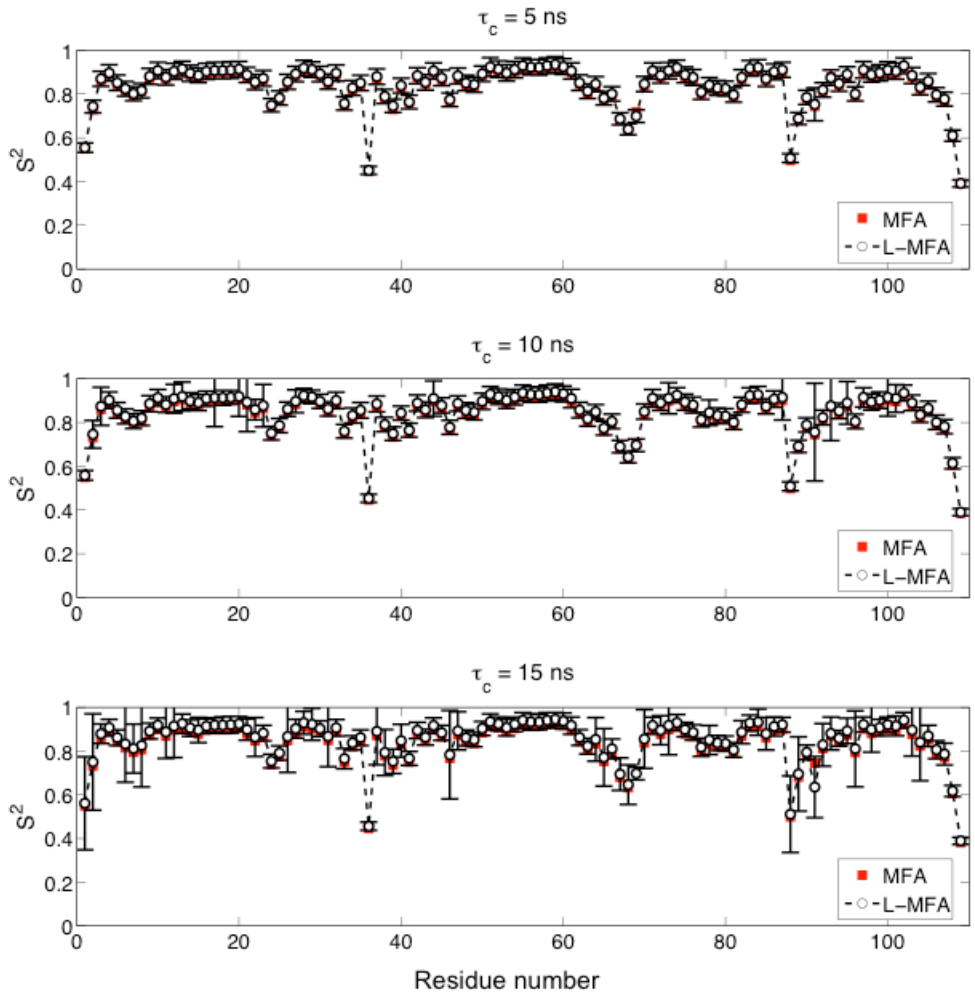

Figure S4. Comparison of S^2 order parameters determined by MFA and L-MFA methods with different τ_c values of 5 ns, 10 ns and 15 ns (from top to bottom). The error bars were estimated by Monte Carlo simulations with 5% errors for R_1 and R_2 values extracted from the MD trajectory (PDB: 1GNU).

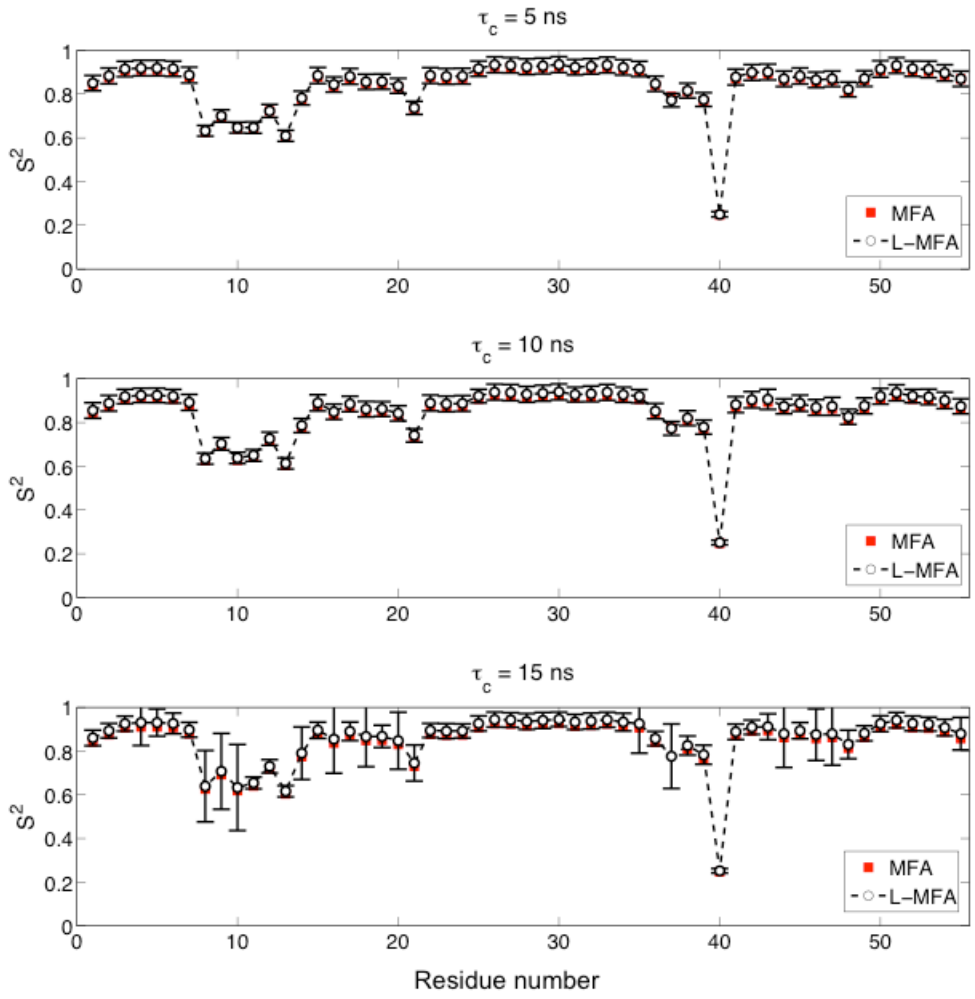

Figure S5. Comparison of S^2 order parameters determined by MFA and L-MFA methods with different τ_c values of 5 ns, 10 ns and 15 ns (from top to bottom). The error bars were estimated by Monte Carlo simulations with 5% errors for R_1 and R_2 values extracted from the MD trajectory (PDB: 1IGD).

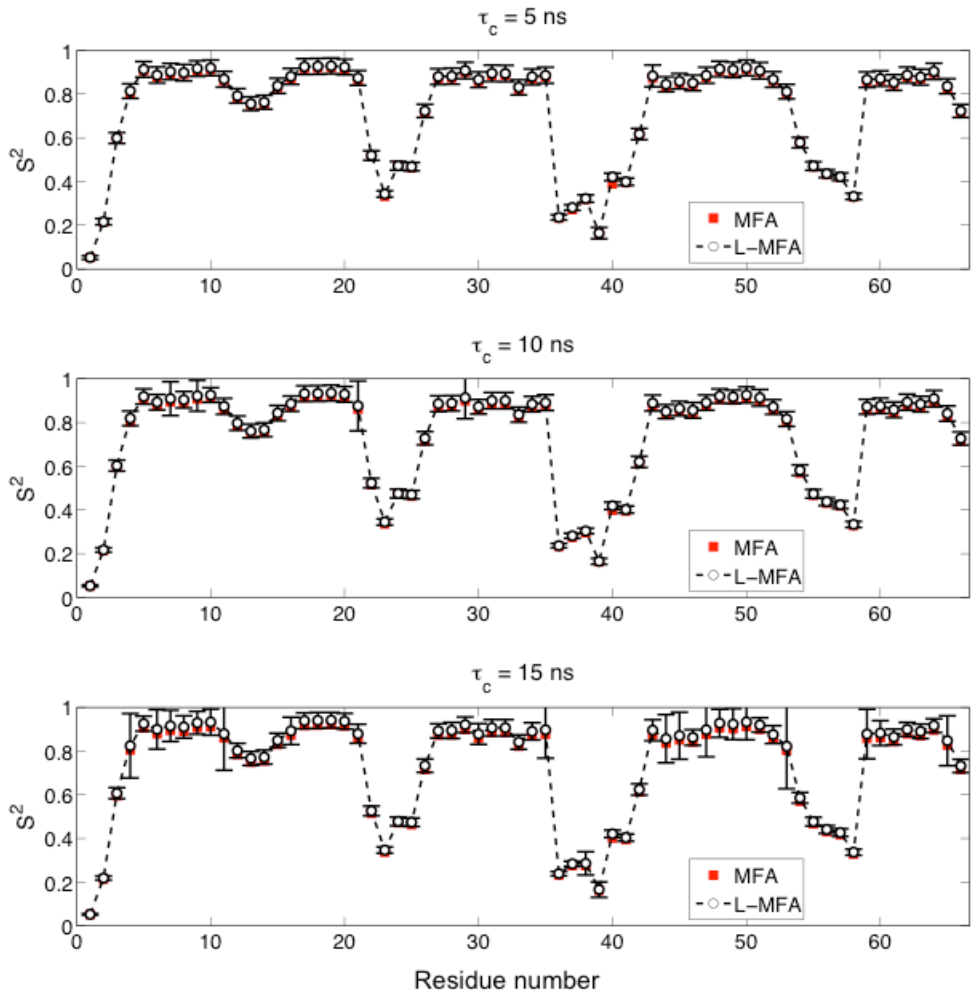

Figure S6. Comparison of S^2 order parameters determined by MFA and L-MFA methods with different τ_c values of 5 ns, 10 ns and 15 ns (from top to bottom). The error bars were estimated by Monte Carlo simulations with 5% errors for R_1 and R_2 values extracted from the MD trajectory (PDB: 1MJC).

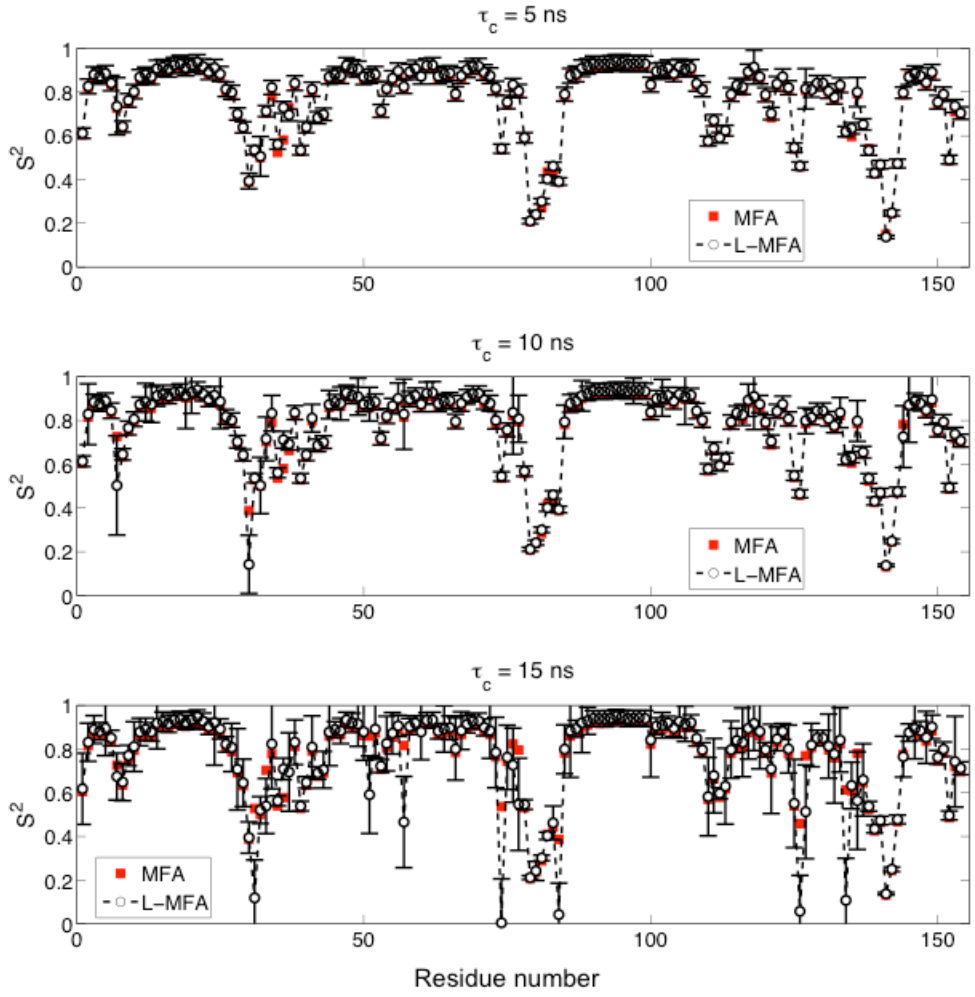

Figure S7. Comparison of S^2 order parameters determined by MFA and L-MFA methods with different τ_c values of 5 ns, 10 ns and 15 ns (from top to bottom). The error bars were estimated by Monte Carlo simulations with 5% errors for R_1 and R_2 values extracted from the MD trajectory (PDB: 1QST).

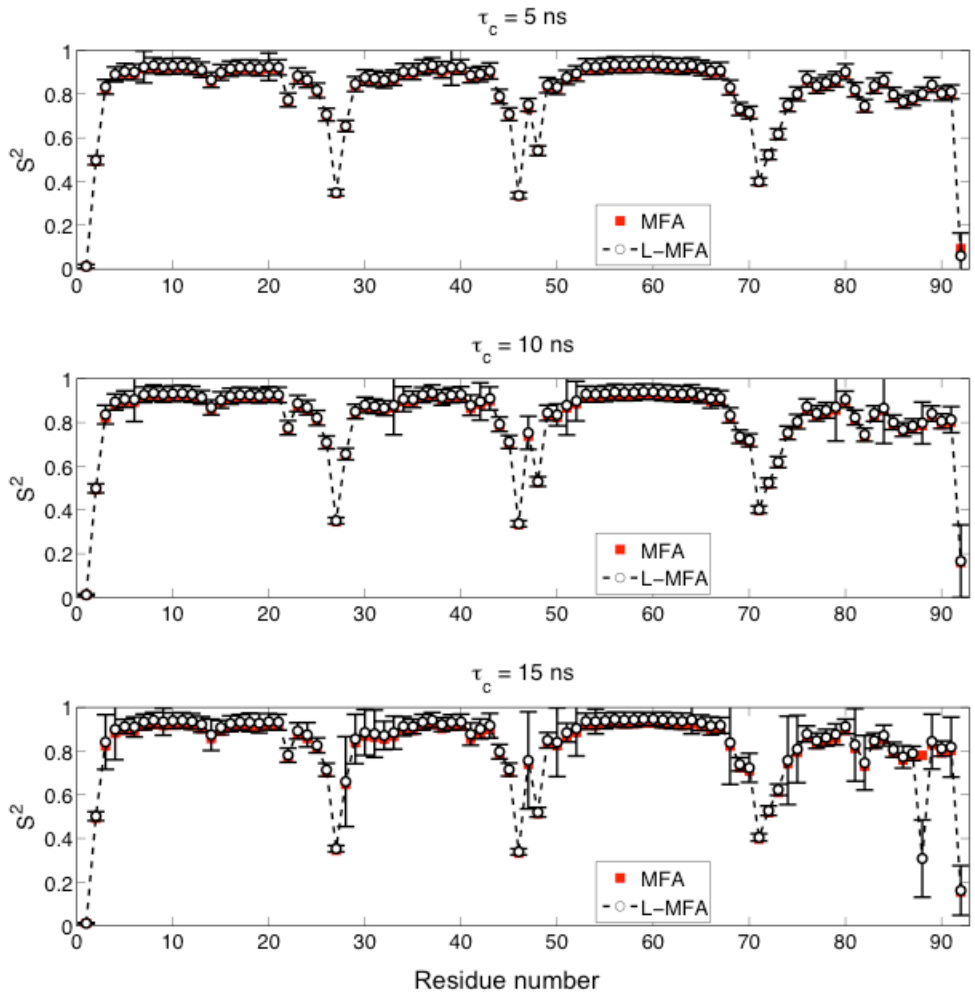

Figure S8. Comparison of S^2 order parameters determined by MFA and L-MFA methods with different τ_c values of 5 ns, 10 ns and 15 ns (from top to bottom). The error bars were estimated by Monte Carlo simulations with 5% errors for R_1 and R_2 values extracted from the MD trajectory (PDB: 1QZM).

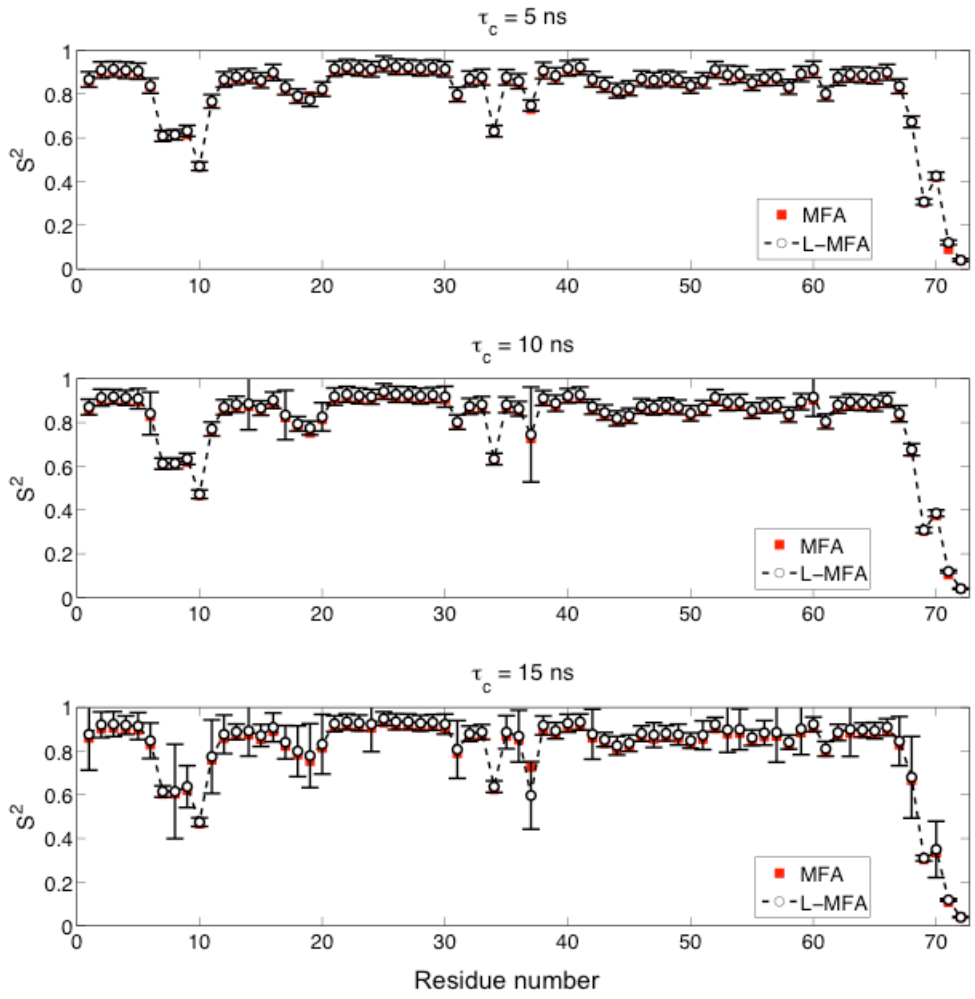

Figure S9. Comparison of S^2 order parameters determined by MFA and L-MFA methods with different τ_c values of 5 ns, 10 ns and 15 ns (from top to bottom). The error bars were estimated by Monte Carlo simulations with 5% errors for R_1 and R_2 values extracted from the MD trajectory (PDB: 1UBI).

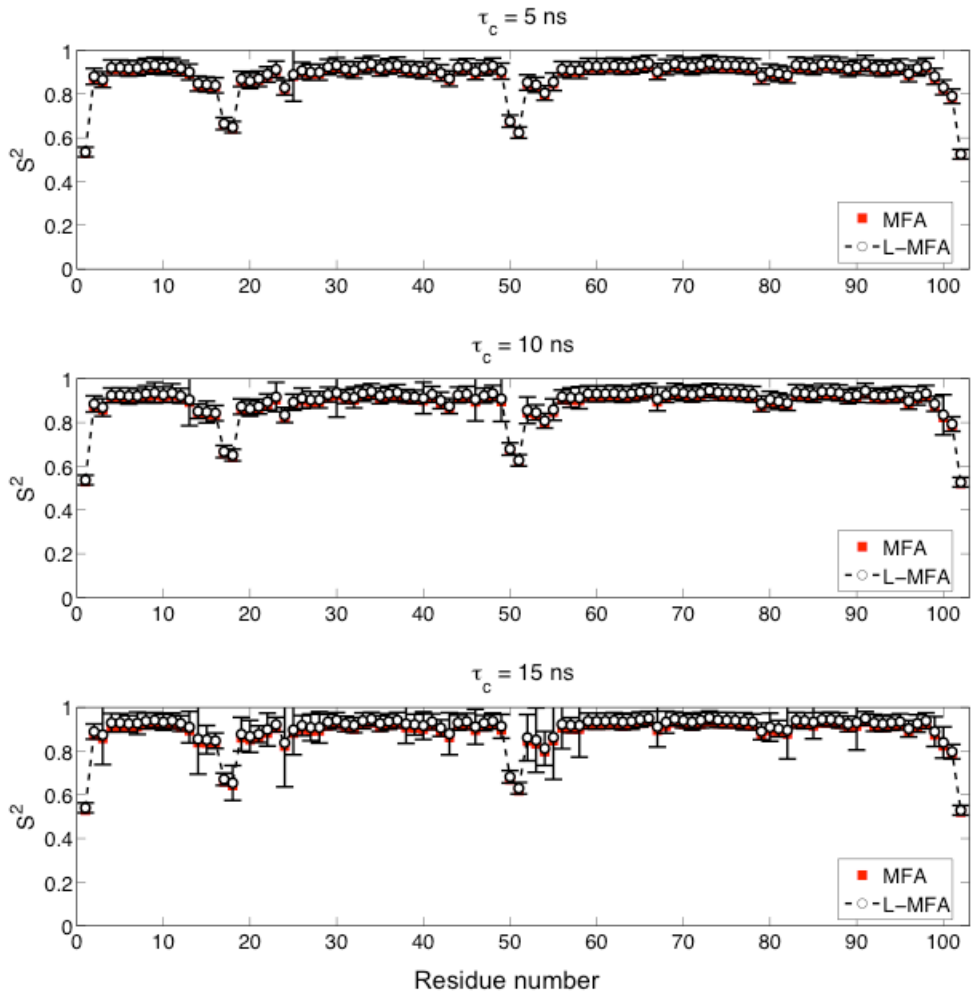

Figure S10. Comparison of S^2 order parameters determined by MFA and L-MFA methods with different τ_c values of 5 ns, 10 ns and 15 ns (from top to bottom). The error bars were estimated by Monte Carlo simulations with 5% errors for R_1 and R_2 values extracted from the MD trajectory (PDB: 1VYK).

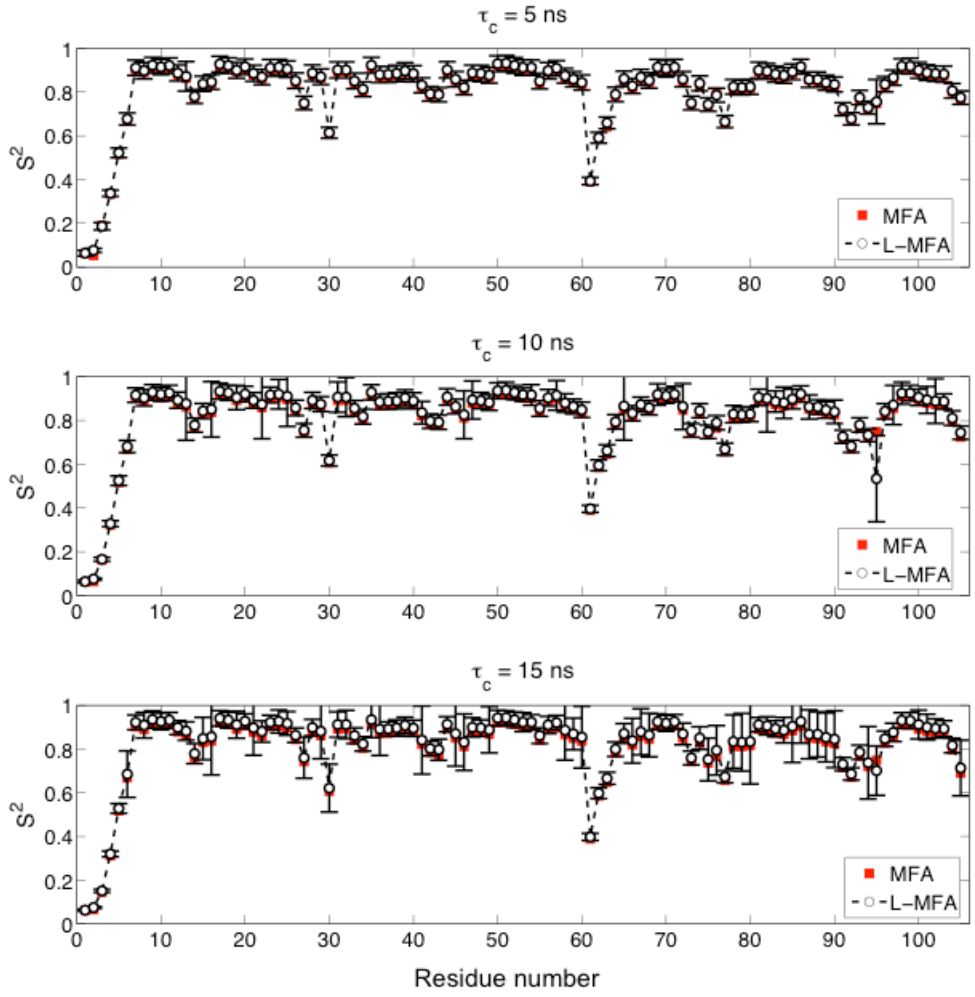

Figure S11. Comparison of S^2 order parameters determined by MFA and L-MFA methods with different τ_c values of 5 ns, 10 ns and 15 ns (from top to bottom). The error bars were estimated by Monte Carlo simulations with 5% errors for R_1 and R_2 values extracted from the MD trajectory (PDB: 2B02).

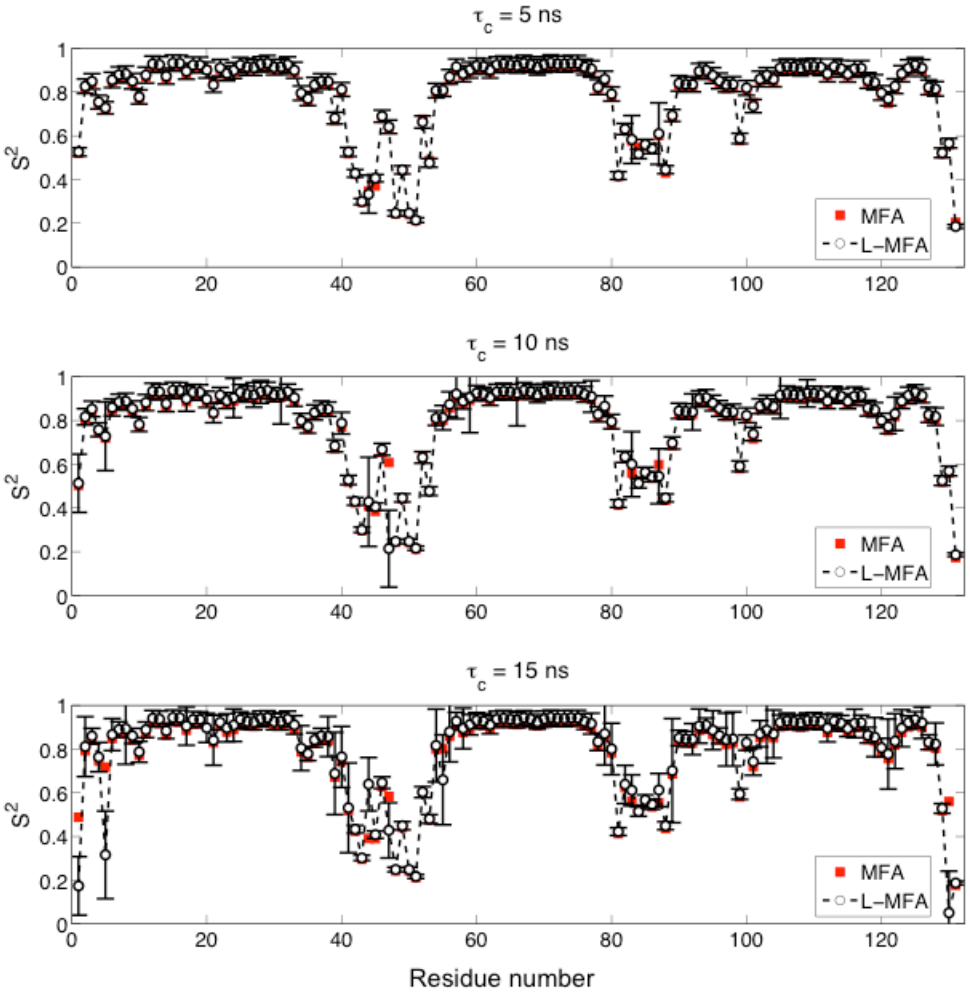

Figure S12. Comparison of S^2 order parameters determined by MFA and L-MFA methods with different τ_c values of 5 ns, 10 ns and 15 ns (from top to bottom). The error bars were estimated by Monte Carlo simulations with 5% errors for R_1 and R_2 values extracted from the MD trajectory (PDB: 2END).

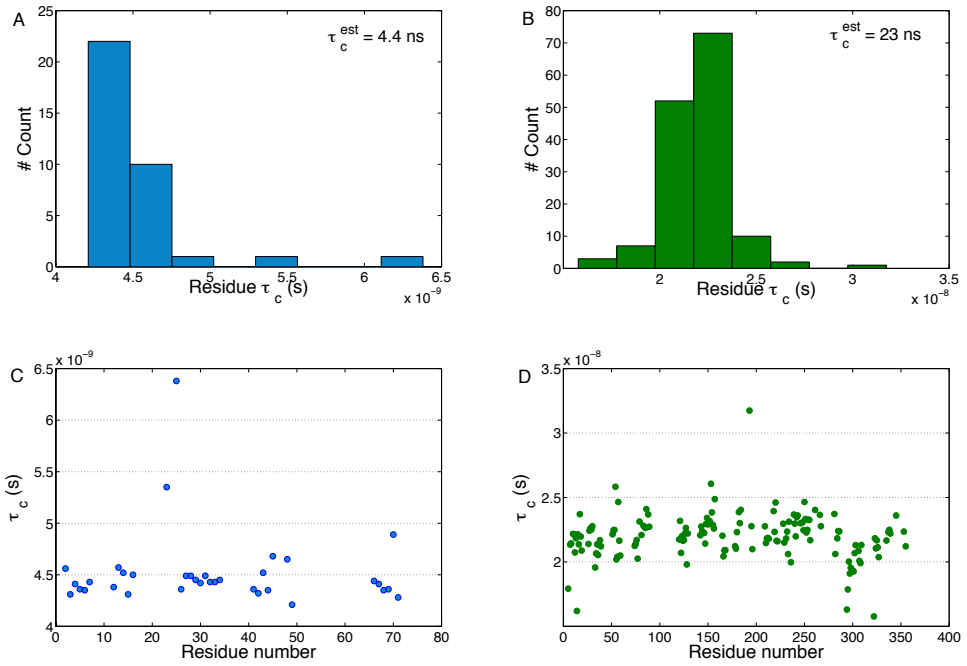

Figure S13. Estimation of global tumbling correlation time τ_c from R_2/R_1 ratios. Histogram of calculated residue-wise τ_c is shown for (A) ubiquitin and (B) AK including only residues belonging to secondary structures according to the DSSP program. The global τ_c values were estimated from the residue-wise τ_c values averaged over all ^{15}N sites that are part of well-defined secondary structures, which results in τ_c values of 4.4 ns and 23 ns for ubiquitin and AK, respectively. The calculated τ_c values from residues in secondary structures are plotted for (C) ubiquitin and (D) AK.

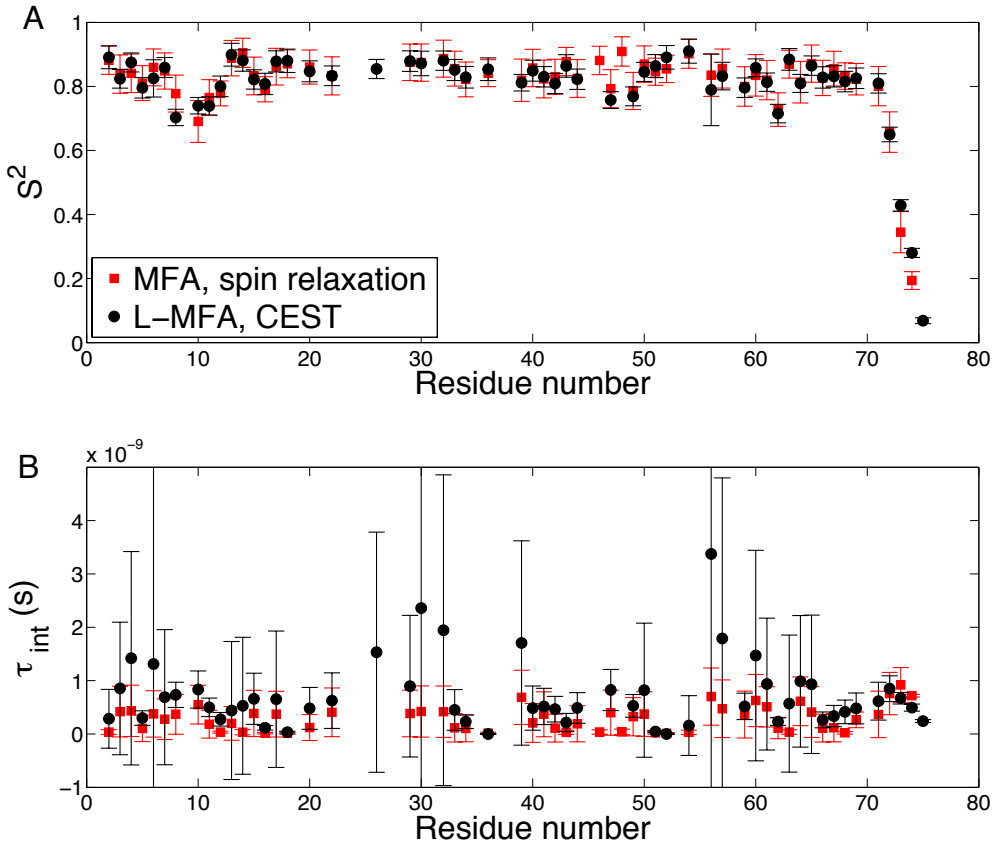

Figure S14. Comparison of ubiquitin S^2 order parameters (A) and internal correlation time τ_{int} (B) extracted by different methods. τ_{int} fitted by MFA of R_1, R_2 and NOE from spin relaxation experiment (red squares). τ_{int} fitted by L-MFA analysis of CEST-derived R_1 and R_2 (black dots). The error bars are estimated from an analysis of 5% Monte Carlo error on relaxation parameters.

References

[1] P. Vallurupalli, G. Bouvignies, L. E. Kay, *J. Am. Chem. Soc.* **2012**, *134*, 8148.
[2] M. Guenneugues, P. Berthault, H. Desvaux, *J. Magn. Reson.* **1999**, *136*, 118.
[3] O. Davulcu, P. F. Flynn, M. S. Chapman, J. J. Skalicky, *Structure* **2009**, *17*, 1356.
[4] F. Delaglio, S. Grzesiek, G. W. Vuister, G. Zhu, J. Pfeifer, A. Bax, *J. Biomol. NMR* **1995**, *6*, 277.
[5] H. M. Mcconnell, *J. Chem. Phys.* **1958**, *28*, 430.
[6] N. A. Lakomek, J. Ying, A. Bax, *J. Biomol. NMR* **2012**, *53*, 209.
[7] M. Gairi, A. Dyachenko, M. T. Gonzalez, M. Feliz, M. Pons, E. Giralt, *J. Biomol. NMR* **2015**, *62*, 209.
[8] A. G. Palmer, 3rd, C. D. Kroenke, J. P. Loria, *Methods Enzymol.* **2001**, *339*, 204.
[9] (a) M. G. Carneiro, J. G. Reddy, C. Griesinger, D. Lee, *J. Biomol. NMR* **2015**, *63*, 237; (b) A. L. Hansen, G. Bouvignies, L. E. Kay, *J. Biomol. NMR* **2013**, *55*, 279.
[10] (a) N. L. Fawzi, J. F. Ying, R. Ghirlando, D. A. Torchia, G. M. Clore, *Nature* **2011**, *480*, 268; (b) P. Vallurupalli, G. Bouvignies, L. E. Kay, *J. Phys. Chem. B* **2011**, *115*, 14891.
[11] Y. Gu, D. W. Li, R. Brüschweiler, *J. Chem. Theory Comput.* **2014**, *10*, 2599.